Hindawi
Advances in Materials Science and Engineering
Volume 2018, Article ID 4206836, 10 pages
https://doi.org/10.1155/2018/4206836

Research Article

Aggregate Evolution Mechanism during Ion-Adsorption Rare Earth Ore Leaching

Kui Zhao,[1,2] Yulong Zhuo,[1,2] Xiaojun Wang,[1,2] and Wen Zhong[1,2]

[1]*Jiangxi Key Laboratory of Mining Engineering, Jiangxi University of Science and Technology, Jiangxi 341000, China*
[2]*School of Resources and Environment Engineering, Jiangxi University of Science and Technology, Jiangxi 341000, China*

Correspondence should be addressed to Yulong Zhuo; 879408217@qq.com and Xiaojun Wang; xiaojun7903@126.com

Received 16 August 2018; Accepted 6 November 2018; Published 21 November 2018

Academic Editor: Ali Nazari

The phenomenon of particle aggregation occurs when ammonium chloride is used as a leaching reagent to infiltrate rare earth samples. To reveal the formation and evolution mechanisms of aggregates, a self-developed column leaching experimental device was employed in conjunction with nuclear magnetic resonance technology. The relationships among the amount of rare earth leaching, the evolution of the microscopic pore structure, the porosity, and the leaching time were obtained. A comparative analysis of pure water and ammonium chloride test groups revealed that aggregates were present only in the latter. Consequently, the results of comprehensive analyses indicate that the formation of aggregates is a temporary particle deposition phenomenon caused by the settling of fine soil particles migrating from the top to the bottom of a sample. Furthermore, chemical exchanges constitute the main cause of aggregate formation.

1. Introduction

Ion-adsorption rare earth ore, also known as weathering shell leaching rare earth ore, was first discovered in a foot cave in Longnan County, Jiangxi Province, in the late 1960s. Ion-adsorption rare earth ore is found in shallow, weathered rock formations [1–5]. Currently, mining is conducted through a relatively mature process known as in situ leaching and mining, which uses mainly chemical exchange reactions composed of a leaching solution during the seepage process of an ore body to recover rare earth cations, thereby extracting rare earth elements [6–9]. The rare earth leaching rate depends on the degree of the chemical exchange and the seepage of the rare earth mother liquor in the ore body. This ion-adsorption rare earth leaching process includes both analytical and antiadsorption processes. The exchange of rare earth cations is performed under dynamic equilibrium conditions. Furthermore, various parameters of the leaching ore body, including the concentration of the leaching solution, the cation activity, and the temperature, are positively related to the intensity of the chemical exchange. A previous experimental study found that the rare earth leaching rate is affected by changes in the microscopic pore structure during the seepage process [10]. Therefore, research on the relationship between the evolution of the pore structure and the leaching rate during the rare earth leaching process is highly significant for the development of green extraction technologies and for the efficient recovery of ion-adsorption rare earth ores.

In recent years, with the extensive use of microcomputed tomography (CT) technology [11–13], scholars worldwide have begun to study the evolution of the microstructures of rock and soil media and their influencing mechanisms. Among those researchers, Kodali et al. used micro-CT to study the distribution of microcracks inside copper ore particles [14]. Similarly, Nosrati et al. used micro-CT to scan the internal structure of granulated nickel ore and reported the distribution of the microscopic structure [15], while Yan et al. introduced microscopic parameters to describe the pore characteristics of soil [16]. Zhuo et al. used nuclear magnetic resonance (NMR) scanning to study the relationship between the pore size distribution and the weakening of the intensity of ion-adsorption rare earth leaching processes, thereby revealing the mechanism through which the ore body strength

becomes weakened during leaching [17, 18]. Wang et al. studied the variations in the permeability characteristics of rare earth ore bodies under seepage-chemical coupling using an indoor column leaching test [10].

The mineral leaching rate, which indicates the extent to which a metal is leached, represents one of the criteria for the leaching processes of various metals. With the continuous expansion of the scale of the production of mineral resources, the grade of infiltration has gradually decreased, and increasing numbers of scholars have initiated research on the mechanisms behind the leaching rate. Xiao et al. proposed the concept of ion-adsorption rare earth ore leaching using magnesium sulfate as a leaching agent from an environmental protection perspective; with a magnesium sulfate concentration of 0.2 mol/L, the rare earth leaching rate can exceed 95% [19]. In addition, Li et al. used citrate as a leaching agent to leach the weathering crust of rare earth ore; they postulated that the coordination of citrate ions with rare earth ions can promote rare earth ion exchanges among ores to increase the rare earth ore recovery rate [20].

During the in situ leaching of ion-adsorption rare earth ores, the pore structure of the ore body changes dynamically with the injection strength and the duration of liquid injection. This series of changes to the pore structure directly affects the permeability characteristics of the ore body. Moreover, the seepage of the leaching solution affects the stability of the slope. Existing research shows that particles experience both migration and blockage during the soil seepage process. However, few reports have been published regarding the disappearance of particles, the relationship between the blockage and disappearance of particles, and the chemical exchanges that occur during the leaching of rare earth ores. Based on NMR technology, this paper studies the evolutionary mechanism of the pore structure during the leaching of rare earth ore bodies and finds the relationship between internal structural changes and the leaching rate of ore bodies. This study also provides an important research basis for the leaching and extraction of ion-adsorption rare earth ores.

2. Experiments

2.1. Materials and Characterization. Rare earth ore samples were taken from a rare earth mine in Longnan County of southern China. The grade of Longnan ion-adsorption rare earth ore is low, mainly in the range of a few thousands. However, rare earth elements, especially heavy rare earth elements, with complete distributions are abundant. Moreover, the content of radioactive elements is low; as a result, most ore deposits are nonradioactive. The rare earth elements are mainly adsorbed onto the surfaces of ionic clay minerals in fully weathered layers.

For the following procedure, we followed the approach of Zhuo et al. [21]. The samples were acquired by collecting rare earth ores from the mine, and the sample sizes coincided with the effective NMR detection area. The diameter-to-height ratio ranged from 40 mm to 60 mm. The soil samples were air-dried before the tests; hence, the water content was 0%. During the remodelling process, the density and moisture content of the original soil samples were maintained to the maximum extent possible, as shown in Figure 1. Each sample was pretested by comparing the densities to determine the appropriate number of compaction events; this number was determined to be 3, and the compaction height was determined to be 30 cm. A standard compaction device with a compaction hammer diameter of 40 mm was employed. After phase detection, the rare earth content of the original sample was determined to be 0.070 ± 0.003%, which conforms to the experimental requirements. The physical parameters of the remodelled rare earth sample are provided in Table 1.

2.2. Chemical Replacement. Rare earth elements are found in strong weathered granites in the form of ions. An NH_4Cl solution is typically used during the leaching process [22, 23]. The rare earth cations adsorbed onto the ore body are replaced by NH_4^+, which has relatively active chemical properties, as shown in Formula (1) [24]. This strong chemical reaction occurs throughout the leaching process. The ion exchange that occurs during leaching involves the adjustment and reconstruction of the mineral microstructure, leading to changes in the crystal structure chain. The seepage effect of the leaching solution also impacts the microstructure of the ore body.

$$\left[Al_4\left(Si_4O_{10}\right)(OH)_8\right]_m \cdot n{RE^{3+}}_{(s)} + 3n{NH_4^+}_{(aq)} = \left[Al_4\left(Si_4O_{10}\right)(OH)_8\right]_m \cdot \left(NH_4^+\right)_{3n(s)} + n{RE^{3+}}_{(aq)}. \quad (1)$$

2.3. Column Leaching Test. The column leaching test device designed and developed in-house is adopted in this study. As shown in Figure 2, the column leaching test device consists of (from top to bottom) the leaching zone, filter paper, remodelled rare earth samples, filter paper, leaking liquid, liquid collection funnel, and liquid collection apparatus. The specific test steps are as follows:

(1) Put the remodelled rare earth sample into the column leaching device. Connect the various parts of the device as shown in Figure 2.

(2) First, saturate the remodelled rare earth sample by injecting 15 mL of pure water into the top of the sample; according to a preliminary test, when the injection volume is 15 mL, a magnetic resonance imaging (MRI) scan can obtain four images encompassing an even distribution of aggregates, which is helpful for constraining the evolution mechanism of aggregates. Based on a preliminary exploratory test, the designed injection rate is 1 mL/min. The process is considered complete if no liquid leakage is observed in the collection funnel within a span of 3 min; subsequently, the rare earth sample is taken for NMR scanning. Record the volume of the recovered liquid and the porosity test results at this time. After the NMR scanning test, repeat the previous steps until the differences between the two recovered liquids and the

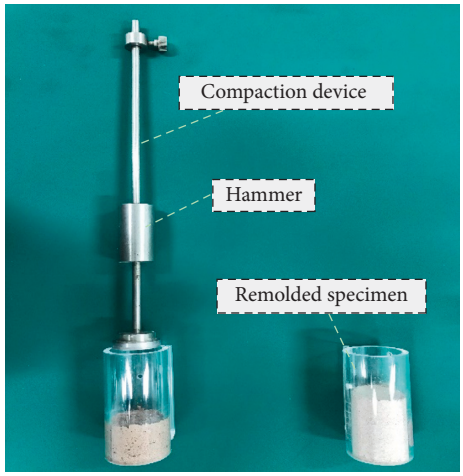

Figure 1: Manufacturing process of the remodelled soil specimens.

Table 1: Physical parameters of the remodelled rare earth ore sample.

Parameter type	Geometric dimensions (mm)		Density (g/cm^3)	Moisture content (%)	Quality (g)
	Diameter	Height			
Value	40	60	1.75	15	113

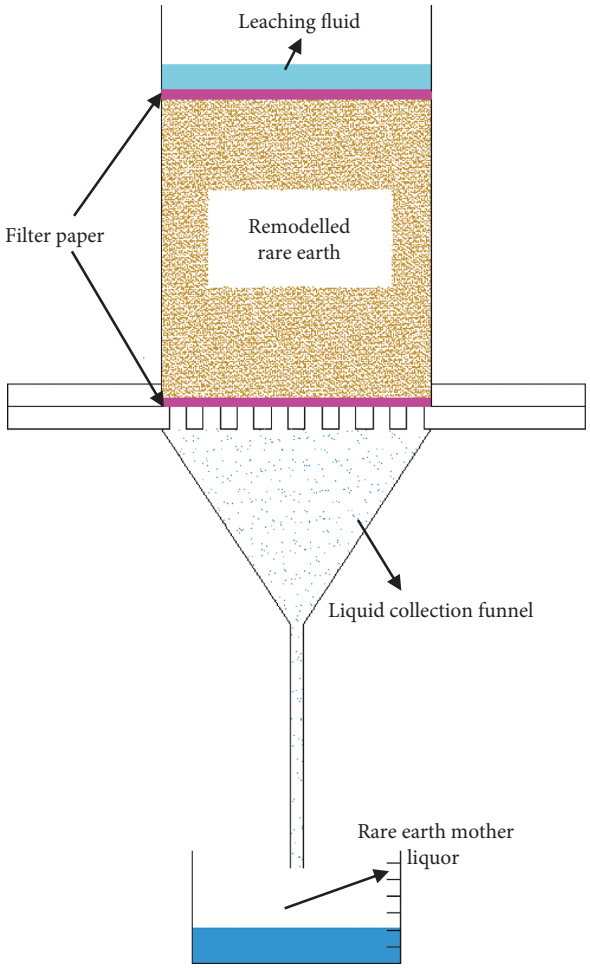

Figure 2: Column leaching test device.

porosity test results are less than 0.1, at which the sample is considered to be saturated.

(3) Begin the leaching test. The samples are divided into two groups: one group has a leaching solution composed of pure water and the other group contains a leaching solution of ammonium chloride. The pH value of the solution is maintained at 6.5. The test procedure is the same as that in step (2), but the criteria marking the end of the experiment are different.

(4) Terminate the experiment. The test is concluded when the leaching of the rare earth ion content cannot be determined by EDTA titration.

2.4. Microstructure Tests. NMR, which constitutes a new type of detection technology, has been widely applied in the field of geotechnical engineering [25]. This technology is most importantly characterized by its ability to rapidly, accurately, and quantitatively measure the microstructure porosity and pore size distribution while keeping the structures of the rock and soil intact (i.e., nondestructive testing). Therefore, NMR represents the most suitable detection technology for an analysis of the microstructural evolution of a rare earth ore body during the leaching process.

The micropore structure of the samples was measured using a PQ-OO1-type Mini-NMR (Suzhou Niumag Analytical Instrument Corporation, Suzhou, China), as shown in Figure 3, in which the permanent magnets possess a magnetic field intensity of 0.52 T. During the experiments, the valid experimental area of the sample was 60 mm × 60 mm, and the temperature of the permanent magnets was kept at 32 ± 0.01°C to ensure the stability and uniformity of the experimental magnetic field. A test sample was obtained after each leaching test. After detection, leaching was performed on the same sample; when detecting the microstructure of a sample, the homogeneity of the sample must be ensured to analyse the microstructural evolution of the rare earth ore body during the leaching process.

2.5. Titration Test. The rare earth ion content in the rare earth mother liquor during the test was determined by titration with disodium EDTA, which constituted the titration reagent. The buffer solution was dissolved in pure water with hexamethylenetetramine, and 10 mL of concentrated hydrochloric acid was added. The masking reagent was composed of 1% sulfosalicylic acid, 5% ascorbic acid, and 5% acetylacetone. Xylene orange was used as the agent. According to national standard GB/T 14635-2008 "Rare earth metals and their compounds: determination of total rare earth contents" in combination with the actual conditions of the mother liquor collected during the test, 5 mL of the rare earth mother liquor was titrated for each experiment. The rare earth ion leaching concentration in the secondary rare earth mother liquor is calculated according to the following formula:

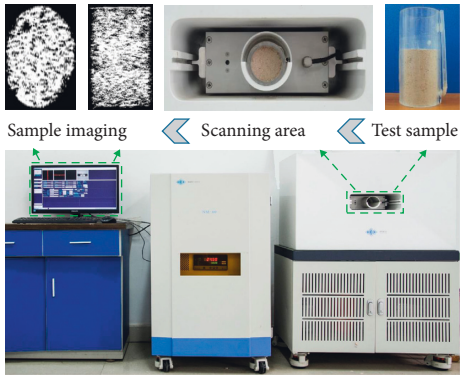

Figure 3: PQ-OO1-type Mini-NMR.

$$C_{RE} = \frac{(C_{EDTA} * (B - A))}{5}, \quad (2)$$

where C_{RE} is the rare earth ion concentration, mL/mg; C_{EDTA} is the titrant standard concentration, mL/mg; B is the burette reading after titration, mL; A is the burette reading before titration, mL; and the denominator of 5 indicates that 5 mL of the rare earth mother liquor is taken.

3. Results and Discussion

3.1. Rare Earth Ion Leaching Rate. Disodium EDTA titration recovery of the rare earth mother liquor was employed to determine the rare earth ion leaching concentration. The leaching quality of rare earth ions was calculated according to the collected volume of rare earth mother liquor. Considering the slight differences in the recovered volume of the mother liquor, the rare earth leaching effect on secondary rare earth ions was characterized by the leaching quality of rare earth ions. According to the results of previous research, pure water does not chemically interact with rare earth ions, indicating that the content of rare earth ions in the mother liquor recovered from a pure water leaching test group should be almost zero [10, 17, 18]. The recovered distribution of the rare earth ion mass from the column leaching test on the samples from the ammonium chloride group is shown in Figure 4, where V_{RE} represents the volume of the recycled rare earth mother liquid.

According to the titration results and the recovered volume of rare earth mother liquor, the quality of each leached rare earth sample was determined. Figure 4 shows the rare earth mass leaching results from the 1st test to the 9th test. The ore leaching process subsequent to the "tail" phenomenon in the rare earth column leaching test (i.e., the leaching qualities following the peak value of the rare earth leaching quality) presents a long duration, and the leaching qualities of the rare earth samples are low. The 8th and 9th leaching rare earth masses shown in Figure 4 are below 1% of the peak mass (the 3rd leaching amount); these leaching times indicate a tail phenomenon [17, 18], and this is not the focus of this study. Overall, the leaching quality of rare earth ions showed either a sharp increase or a sharp drop, and no rare earth leaching occurred during the initial leaching stage. The peak rare earth leaching quality was observed after the

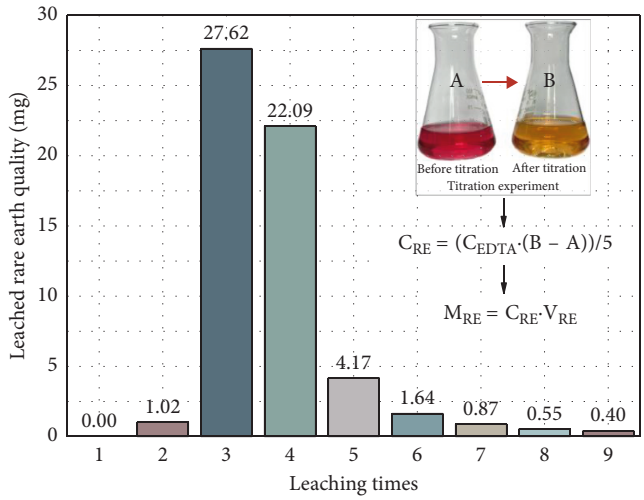

Figure 4: Recovery of the rare earth mass ion distribution.

third and fourth leaching iterations, and the combined rare earth quality of these two leaching processes was 49.71 mg, reaching 71% of the total rare earth content of the sample (a single rare earth sample with a rare earth content of approximately 70 mg was measured in the prior period). After the fourth test, the amount of rare earth leaching decreased significantly, and a tail phenomenon occurred after the eighth leaching iteration.

3.2. Aggregate Phenomenon and Its Components. By analysing the NMR inversion imaging results from a large number of column leaching test samples, the inversion imaging pattern of the sample showed no obvious change with an increase in the infiltration time when the infiltration liquid was composed of pure water. In contrast, when the infiltration liquid was ammonium chloride, sample particles (called aggregates in this article) appeared and migrated from the top to the bottom (the dark areas in Figure 5), and they disappeared from the top down with an increase in the leaching time. All samples for this test were saturated prior to testing to consider differences in the seepage velocities of the samples. The test was considered complete when 15 mL of the leaching solution thoroughly flowed through the soil sample into the mother liquor collection container. Inverted images of the sample obtained when leaching pure water with ammonium chloride are shown in Figure 5. Because this article mainly addresses the presence of aggregates, only the leaching iterations with aggregates up to their disappearance are displayed in Figure 5, and two images after the aggregates disappeared are also given to demonstrate that no aggregates appeared in follow-up leaching iterations.

As shown in Figure 5, aggregates exist only in the sample group in which the leaching solution is ammonium chloride, and they appear only in the first four leachings. After the fourth leaching, the aggregates almost disappear and do not reappear. Moreover, aggregates are not observed in the pure water leaching test group. The red arrows in Figure 5 indicate the movement of the aggregates throughout the leaching process. During the initial stage of infiltration of the

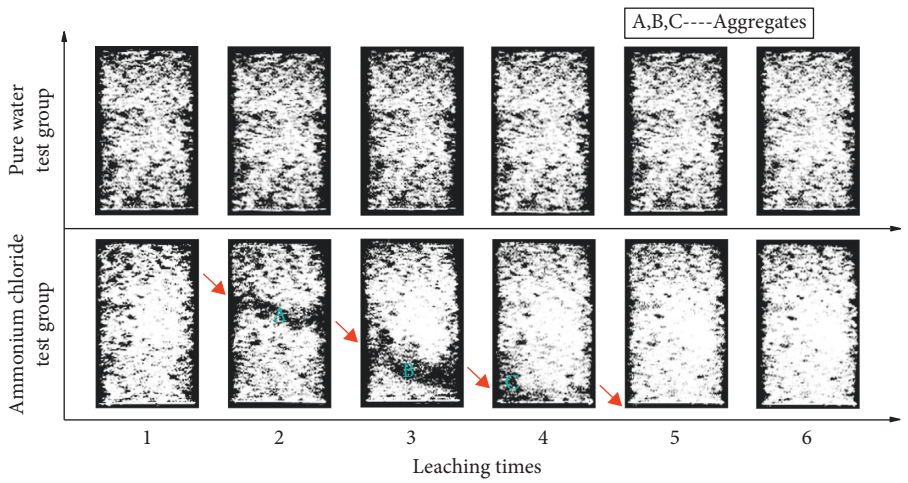

Figure 5: Inversion images of the sample during the column leaching tests.

leaching solution, the aggregates are concentrated mainly near the surface of the liquid leaching solution in the upper part of the sample. With the continuous infiltration of the leaching solution, the aggregates move to the middle of the sample and become readily visible following the completion of the second leaching test. After the third leaching, the aggregates move to the bottom of the adjacent specimen; the amount of aggregates has significantly increased since the previous leaching. After the fourth leaching, the aggregates mostly disappear and remain only in the peripheral part of the sample. In subsequent experiments, no aggregates are discernible, and the image formation of the ammonium chloride group is whiter than that of the pure water group. Furthermore, the pure water group specimens show no change from the beginning to the end of the image, and the black and white areas are staggered.

According to the MRI scanning results, the aggregates within the leaching sample were selected for electron microscopy and energy spectrum analysis. The test results from a comparative analysis and random selection of the original soil samples are shown in Table 2 and Figure 6. Figure 6(a) shows that the rare earth particles are distributed in layers and have a greater number of pores, thereby increasing the specific surface area and improving the clay adsorption capacity. Figures 6(b)–6(d) show that the aggregates include a large number of solid particles. Brighter regions indicate that the particles are densely packed, while darker regions indicate that the degree of particle aggregation is relatively low, indicating that the aggregate region is not characterized by a discernible distribution.

Based on the degree of aggregation of solid particles, the energy spectrum was randomly selected, and the mean elemental mass percent distributions of the original soil samples containing common clay constituent elements, such as carbon, oxygen, aluminium, and silicon, were obtained, and the results are shown in Table 2 and Figure 7. Among the constituent elements, oxygen, aluminium, and silicon account for relatively large proportions. The main components of the aggregates in areas A, B, and C are carbon, oxygen, aluminium, and silicon; these elements represent substantial portions of the clay particles. In other words, the aggregates are not a new material, rather, they constitute large agglomerations of local silting phenomena caused by the obstructed migration of clay particles.

By comparing the original soil samples with the aggregate element distributions from areas A, B, and C, it is relatively evident that the scandium, yttrium, and lanthanum contents in the solid particles within the aggregate region are almost zero, while the contents of the other elements are essentially equivalent. The cations among the rare earth elements can be exchanged with ammonia ions, pulling them from the solid particles into the solution. Therefore, the agglomerated microparticles first chemically exchange cations with the ammonia ions in the solution and then migrate downward under the effect of percolation as the solution moves from the top down.

According to other research findings [26], soil samples experience the migration of particles during water infiltration. However, no obvious aggregates were observed in the pure water infiltration test sample, whereas the aggregates were obvious in the ammonium chloride test group and were present in all of the samples, indicating that simple seepage was not the main cause of aggregate formation.

3.3. Microscopic Pore Characteristics of the Samples. The ratio of pores within a certain radius of a sample to the total number of pores is called the ratio of the pore radius. The distributions of pore radii of different sizes can reflect changes in the microscopic pore structure of a sample during the infiltration of the leaching solution. Accordingly, the T_2 spectrum is used to detect the proportion of each site within the sample through a predetermined spot. The size of the T_2 spectrum is positively related to the pore size; that is, the distribution of the T_2 spectrum can be used to characterize the pore distribution of the sample. To better reveal the aggregate formation mechanism, the T_2 spectrum distributions with pure water and ammonium chloride as the leaching solutions are shown in Figure 8, in which the 0th time indicates the initial pore distribution when the sample is saturated.

Table 2: Elemental mass percent distribution at each measuring point.

Spectrum	C	O	Al	Si	Fe	La	Ce	Nd
(a) Mass percent distribution of the original soil sample								
360	5.19	51.13	9.14	20.08	—	1.23	2.89	0.17
361	6.80	36.48	13.67	29.99	—	—	—	0.17
362	9.80	56.99	10.75	15.84	—	—	—	—
363	4.71	63.45	16.22	14.43	0.44	—	—	—
364	5.27	59.17	15.98	14.80	0.61	—	1.36	0.06
365	—	56.17	21.60	20.06	1.18	—	—	—
366	7.09	59.27	18.36	14.90	—	—	—	—
Mean value:	6.48	54.66	15.10	18.58	0.74	1.23	2.12	0.13
Sigma:	1.89	8.84	4.31	5.59	0.38	0.00	1.08	0.07
Sigma mean:	0.71	3.34	1.63	2.11	0.14	0.00	0.41	0.02
	C	O	Al	Si	Fe			
(b) Mass percent distribution of spot soil sample A								
353	7.61	59.00	17.38	15.74	0.26			
354	7.13	56.94	18.87	17.05	—			
355	5.09	56.26	20.20	18.44	—			
356	5.52	60.24	17.75	16.49	—			
357	6.30	55.94	19.71	18.04	—			
358	6.79	58.46	18.50	16.01	0.25			
359	5.71	52.87	21.68	19.73	—			
Mean value:	6.31	57.10	19.16	17.36	0.25			
Sigma:	0.92	2.43	1.50	1.45	0.01			
Sigma mean:	0.35	0.92	0.57	0.55	0.00			
(c) Mass percent distribution of spot soil sample B								
346	5.92	59.36	15.38	19.25	0.08			
347	6.34	60.93	13.04	18.66	1.02			
348	5.08	56.91	22.14	15.84	0.03			
349	5.61	60.20	16.07	16.86	1.25			
350	5.59	58.79	14.89	20.66	0.06			
351	6.84	55.61	16.47	17.21	3.86			
352	5.68	58.59	16.33	19.28	0.15			
Mean value:	5.87	58.63	13.32	18.25	0.92			
Sigma:	0.57	1.84	4.30	1.68	1.39			
Sigma mean:	0.22	0.69	1.62	0.63	0.52			
(d) Mass percent distribution of spot soil sample C								
339	6.27	52.49	16.68	24.55	—			
340	8.12	54.26	18.28	19.33	—			
341	6.57	56.3	15.44	21.68	—			
342	7.35	55.26	16.99	20.39	—			
343	5.84	63.19	11.24	19.39	0.33			
344	6.38	56.57	18.65	18.39	—			
345	7.47	63.96	11.97	16.59	—			
Mean value:	6.86	57.43	15.61	20.04	0.33			
Sigma:	0.81	4.42	2.94	2.54	0.00			
Sigma mean:	0.30	1.67	1.11	0.96	0.00			

To facilitate this analysis, the area with T_2 spectrum values of less than 1 ms is defined as pore A, the area with T_2 spectrum values between 1 ms and 10 ms is defined as pore B, the area with T_2 spectrum values between 10 ms and 100 ms is defined as pore C, the area with T_2 spectrum values between 100 ms and 1000 ms is defined as pore D, and the area with T_2 spectrum values greater than 1000 ms is defined as pore E; the pore areas increase sequentially from A to E. Figures 8(a) and 8(b) show that the initial pore distributions of the sample are approximately the same; in addition, a trend is observed where two small central areas become one large area. At the end of the first leaching, the overall pore size distributions of the two groups of specimens did not change significantly. The changes were mainly concentrated in regions D and E, and there was a shift from region E to region D. Specifically, the diameters of some large-diameter pores decreased. At the end of the second and third leachings, the two groups of samples continued to follow the trend of a reduction in the diameters of large-diameter pores, and the trend of the change in the pore size of the ammonium chloride group sample was significantly stronger than that of the pure water group sample. After the fourth leaching of the pure water group sample, the pore size of each area fluctuated in a small range; that is, the pore size tended to be roughly constant. In contrast, after the fourth leaching of the ammonium chloride group sample, the numbers of small-diameter pores in areas B and C greatly diminished, while the numbers of large-diameter pores in those areas greatly increased; subsequently, the pore diameters in the various leaching regions also tended to remain approximately constant. The pore size distribution for the overall leaching process can be divided into two stages: a dynamic change period and a quiet period. Studies [25] have shown that changes in the sample skeleton, particle generation, and migration are all important causes of variations in the pore diameter.

The micropore structures of the samples were measured using a PQ-OO1-type Mini-NMR. After the test, various pore radius distributions were determined. The sum of the ratios of the pore radius for each size is called the porosity of the sample. The error of the NMR test results is ±1%; therefore, to reduce the influence of instrumental errors on the test results, each test was performed thrice (i.e., 3 measurements were obtained) to provide an arithmetic average for the porosity of the test sample. Considering the influence of the expansion of the soil samples on the test analysis, the height of each sample was measured before each test, and the height of the sample was measured four times before the test along the wall surface of the device. The average value was taken as the average height of the test sample. During the test, the soil sample did not slide along the inner tube wall. Furthermore, there was no gap between the soil sample and the inner wall of the device. In addition, because the column leaching test device is composed of an acrylic sheet, the diameter of the device did not change during the test, which means that the soil sample was fixed in the radial direction with a constrained size of 50 mm. The specific physical parameters and porosities of the samples are shown in Table 3.

Table 3 shows that the volumes of the two groups of samples remained unchanged after the onset of leaching (i.e., subsequent to the initiation of the first leaching). The initial porosities of the samples (referred to as the 0th time before the first experiment) were basically equivalent. With an increasing number of leachings, the porosities of both samples gradually increased, but the increase in the porosity of the pure water sample was small, and no obvious growth in the porosity was observed. The overall increase in the porosity of the ammonium chloride sample was significantly higher than that of the pure water sample, and the porosities after the first, second, third, and fourth leachings exhibited large increases; after subsequent leachings, however, the

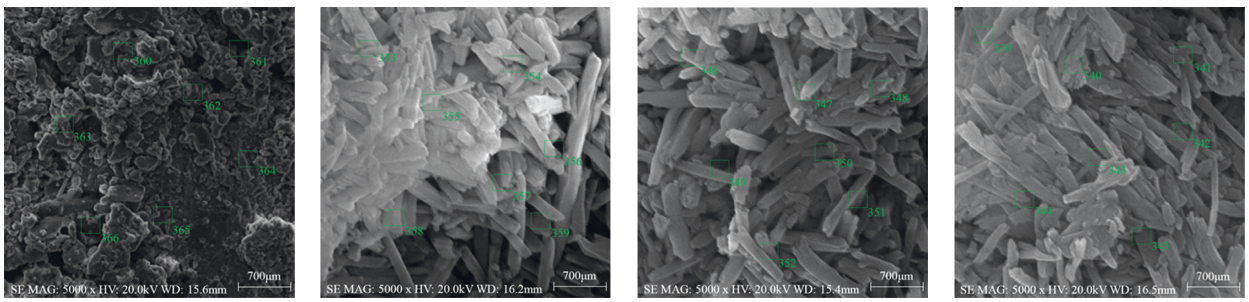

(a) (b) (c) (d)

Figure 6: Layout of spectral scanning measurement points of the soil samples. (a) Original. (b) Spot A. (c) Spot B. (d) Spot C.

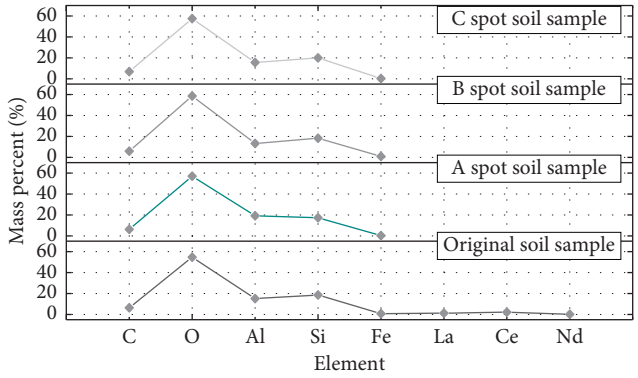

Figure 7: Elemental mass percent distribution.

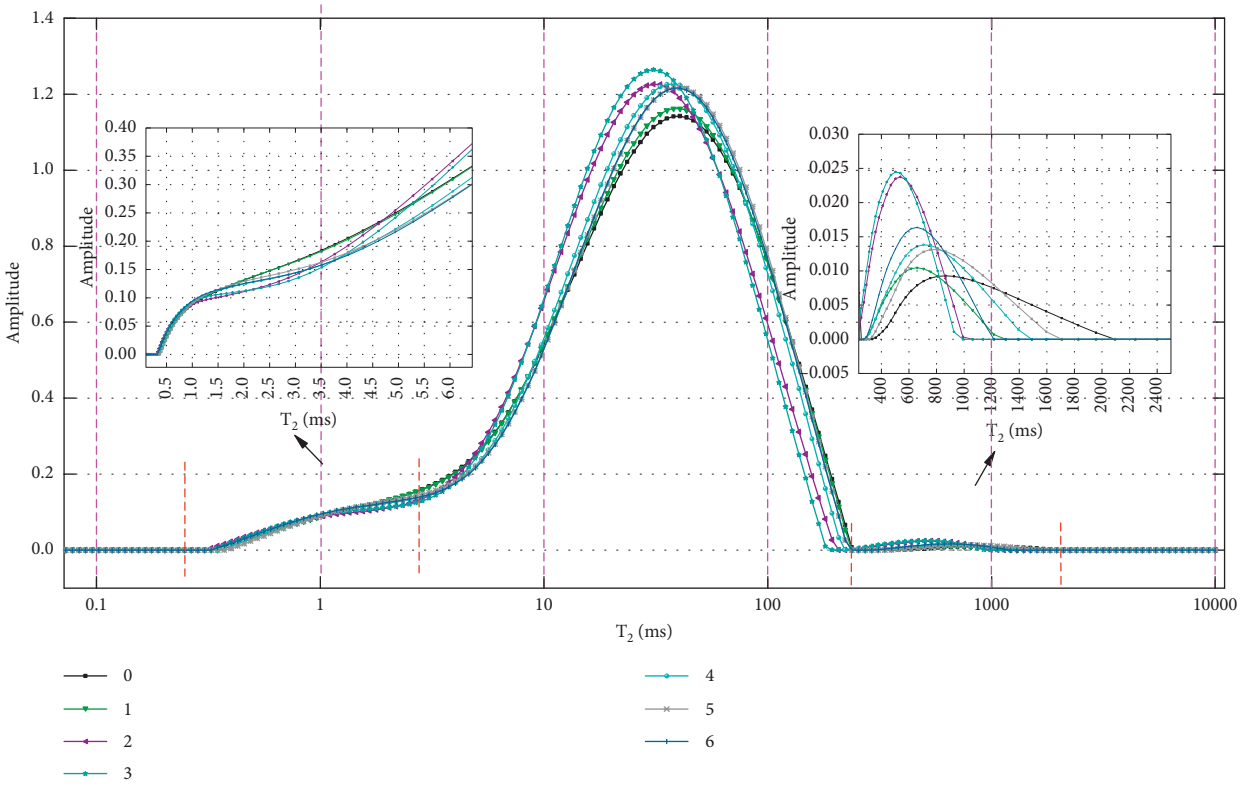

(a)

Figure 8: Continued.

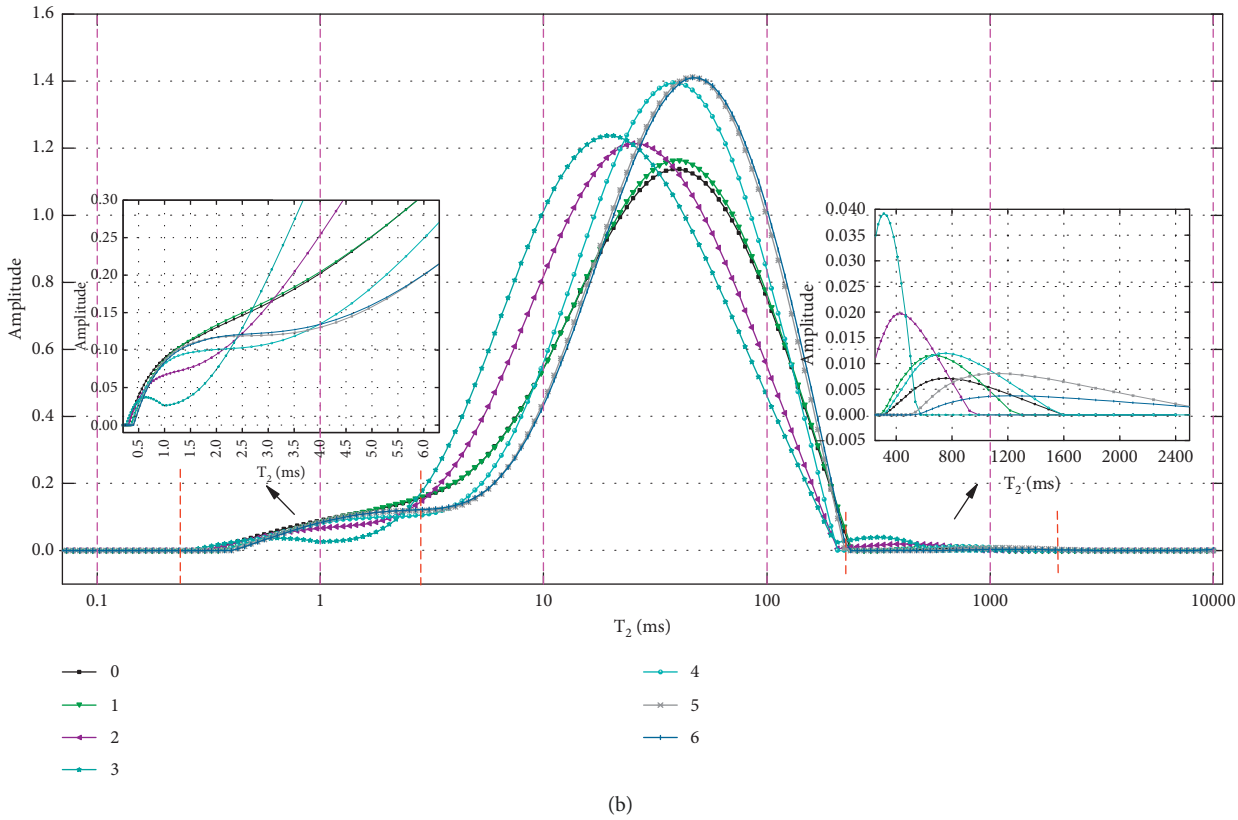

(b)

Figure 8: Sample leaching T_2 spectrum distributions. (a) Pure water leaching T_2 spectrum distribution. (b) Ammonium chloride leaching T_2 spectrum distribution.

Table 3: Physical parameters and porosity distributions of the samples.

Frequency	Sample height (mm)					Volume (mm^3)	Porosity (%)			
	Test 1	Test 2	Test 3	Test 4	Average value		Test 1	Test 2	Test 3	Average value
(a) Pure water leaching test group										
0	59	59	60	60	59.5	74.732	45.116	45.443	45.437	45.332
1	59	60	59	60	59.5	74.732	45.683	45.653	45.663	45.666
2	59	59	60	60	59.5	74.732	45.880	45.783	45.764	45.809
3	59	59	60	60	59.5	74.732	45.653	45.862	45.443	45.652
4	59	59	60	60	59.5	74.732	45.880	46.081	46.153	46.038
5	59	59	60	60	59.5	74.732	46.235	45.879	46.545	46.230
6	59	59	60	60	59.5	74.732	46.503	45.667	46.259	46.143
(b) Ammonium chloride leaching test group										
0	58	59	59	58	58.5	73.476	45.258	45.392	45.267	45.305
1	59	60	58	59	59	74.104	45.919	45.880	46.004	45.934
2	58	60	59	59	59	74.104	47.458	47.562	47.498	47.506
3	59	59	59	59	59	74.104	48.767	48.971	48.908	48.882
4	58	60	59	59	59	74.104	49.711	49.906	49.011	49.542
5	59	60	59	58	59	74.104	49.968	49.083	49.784	49.612
6	59	60	59	58	59	74.104	49.544	49.899	49.568	49.670

porosity fluctuated only within a certain range. The constant volume of the ammonium chloride sample indicates that there was no significant change in the overall support skeleton within the sample during the leaching process, and the increase in the porosity was a result of the combined effect of seepage and chemical exchanges in addition to the ionic strength and viscosity. In contrast, the change in the porosity during pure water leaching was not significant, indicating that seepage was not the main cause of the increase in the porosity.

3.4. Aggregate Formation Mechanism and Its Effect on the Leaching Rate. Aggregates existed only in the ammonium

chloride leaching group, and the aggregates began to germinate at the end of the first leaching. The presence of aggregates was the most significant after the second, third, and fourth leachings, and the ion leaching amount peaked during those times. However, after the fourth leaching, aggregates no longer appeared, and the ion leaching rate decreased sharply, indicating that the strong ion exchange effect is closely related to the production of aggregates. In combination with the pore distribution and the changes in the porosity of the ammonium chloride sample, the strong chemical exchanges did not affect the main support skeleton of the soil sample. However, under the combined effect of seepage and chemical exchanges in addition to the ionic strength and viscosity, a large number of fine clay particles and large particles were removed and transferred into the solution. With the sharp increase in the fine particle content, the original seepage flow channels became congested. Over time, the particles gradually aggregated to form the black areas of aggregation shown in Figure 5. The decrease in ion leaching observed upon comparing the ammonium leaching before and after the leaching of the ammonium chloride group sample indicates that the exchange effect was weakened, the changes in the pore distribution and porosity tended to become stable, and the aggregates disappeared. This strong degree of chemical exchange is an indispensable factor in the formation of aggregates, while the ionic strength and viscosity are not the main causes of aggregate formation.

During the initial stage of aggregate formation, the interior of the sample was saturated with water. At this time, the ammonium chloride solution squeezed pure water out from inside the sample, and no rare earth ions were leached. At the end of the second leaching, the aggregates had migrated to the middle of the sample, and the amount of rare earth leaching was reduced. After the third and fourth leachings, the aggregates had reached the bottom of the sample, and the aggregates were leached with large amounts of rare earth ions. At this time, the amount of rare earth leaching peaked, accounting for 71% of the total amount of leaching. This demonstrates that the upper and lower adjacent areas of the aggregates contained large amounts of rare earth ions.

4. Conclusions

(1) No exchange reactions occurred, and no aggregates were produced between the pure water and rare earth ions. The porosity did not change significantly during the process of pure water seepage.

(2) When ammonium chloride was leached, fine soil particles were removed from the large granular soil by chemical exchanges and were transferred into the solution. This process was partially blocked by seepage during migration from the top to the bottom of the sample, resulting in the formation of aggregates. As the number of leachings increased, the aggregates continued to migrate downward.

(3) In the third and fourth test leachings, the amounts of leached rare earth ions were significantly greater than those at other times. The amount of rare earth leaching peaked at the third leaching iteration. This is because the aggregates had reached nearly the bottom of the sample during the third leaching, and thus, the chemical reaction is more complete. After the third leaching, the amount of leaching continuously decreased.

Data Availability

The data used to support the findings of this study are included within the article.

Conflicts of Interest

The authors declare that they have no conflicts of interest.

Authors' Contributions

K.Z and Y.L.Z. conceived and designed the experiments, analysed the data, and wrote the paper. X.J.W. and W.Z. performed most of the experiments and analysed the data.

Acknowledgments

This research was financially supported by the National Natural Science Foundation of China (nos. 51564012 and 51504102), the Science and Technology Project funded by the Education Department of Jiangxi Province (GJJ150653), the Qingjiang Excellent Young Talents of Jiangxi University of Science and Technology, and the Jiangxi University of Science and Technology Excellent Doctoral Thesis Training Project (YB2017001).

References

[1] T. S. Qiu, D. M. Zhu, X. H. Fang, Q. H. Zeng, G. K. Gao, and H. L. Zhu, "Leaching kinetics of ionic rare-earth in ammonia-nitrogen wastewater system added with impurity inhibitors," *Journal of Rare Earths*, vol. 32, no. 12, pp. 1175–1183, 2014.

[2] K. Sanematsu, Y. Kon, A. Imai et al., "Geochemical and mineralogical characteristic of ion-adsorption type REE mineralization in Phuket, Thailand," *Mineralium Deposita*, vol. 48, no. 4, pp. 437–451, 2013.

[3] L. Zhang, K. X. Wu, L. K. Chen, P. Zhu, and Y. H. Ou, "Over view of metallogenic features of ion-adsorption type REE deposits in southern Jiangxi Province," *Journal of the Chinese society of rare earths*, vol. 1, p. 10, 2015.

[4] J. Li, C. Y. Li, B. W. Li, S. B. Wang, J. C. Han, and J. L. Wang, "Acid leaching of low grade rare earth concentrate by microwave heating," *Chinese Journal of Rare Metals*, vol. 38, no. 5, p. 839, 2014.

[5] R. A. Chi, Z. J. Li, C. Peng, G. C. Zhu, and S. M. Xu, "Partitioning properties of rare earth ores in China," *Rare Metals*, vol. 24, no. 3, p. 205, 2005.

[6] Q. B. Zhang, Y. X. Hua, C. Y. Xu et al., "Non-haloaluminate ionic liquids for low-temperature electrodeposition of rare-earth metals-A review," *Journal of Rare Earths*, vol. 33, no. 10, pp. 1017–1025, 2015.

[7] L. Zhao, Z. Dong, G. L. Ma, and W. J. Yuan, "Solution extraction of several lanthanides from nitric acid with is ohexyl-BTP

in [Cnmim][NTf_2] ionic liquid," *Journal of Rare Earths*, vol. 33, no. 11, pp. 1182–1188, 2015.

[8] X. Q. Sun, Y. Ji, J. Chen, and J. T. Ma, "Solvent impregnated resin prepared using task-specific ionic liquids for rare earth separation," *Journal of Rare Earths*, vol. 27, no. 6, pp. 932–936, 2009.

[9] R. X. Wang, B. Y. Xie, P. Yu et al., "Selection of leaching agent and optimization of column leaching process of ion-absorbed rare earth deposits," *Chinese Journal of Rare Metals*, vol. 39, no. 11, pp. 1060–1064, 2015.

[10] X. J. Wang, Y. L. Zhuo, S. Q. Deng et al., "Experimental research on the impact of ion exchange and infiltration on the microstructure of rare earth orebody," *Advances in Materials Science and Engineering*, vol. 2017, Article ID 4762858, 8 pages, 2017.

[11] J. Dewanckele, T. De Kock, M. A. Boone et al., "4D imaging and quantification of pore structure modifications inside natural building stones by means of high resolution X-ray CT," *Science of The Total Environment*, vol. 416, no. 2, pp. 436–448, 2012.

[12] J. R. Kyle and R. A. Ketcham, "Application of high resolution X-ray computed tomography to miner-al deposit origin, evaluation, and processing," *Ore Geology Reviews*, vol. 65, no. 4, pp. 821–839, 2015.

[13] L. J. Munkholm, R. J. Heck, and B. Deen, "Soil pore characteristics assessed from X-ray micro-CT derived images and correlations to soil friability," *Geoderma*, vol. 181-182, no. 7, pp. 22–29, 2012.

[14] P. Kodali, N. Dhawan, T. Depci et al., "Particle damage and exposure analysis in HPGR crushing of selected copper ores for column leaching," *Minerals Engineering*, vol. 24, no. 13, pp. 1478–1487, 2011.

[15] A. Nosrati, K. Quast, D. F. Xu et al., "Agglomeration and column leaching behaviour of nickel laterite ores: effect of ore mineralogy and particle size distribution," *Hydrometallurgy*, vol. 146, no. 5, pp. 29–39, 2014.

[16] X. Q. Yan, Y. G. Fang, and P. Zhang, "Experiment study on the effects of bentonite on the micropore structure characteristics of soil," *Chinese Journal of Geotechnical Engineering*, vol. 33, no. 8, pp. 1302–1307, 2011.

[17] Y. L. Zhuo, X. J. Wang, S. R. Cao et al., "Study on relationship between pore structure and strength weakening of rare earth ore under seepage," *Gold Science and Technology*, vol. 25, no. 5, pp. 101–106, 2017.

[18] Y. L. Zhuo, X. J. Wang, K. Zhao et al., "Study on strength weakening mechanism of iron-adsorbed rare earth ore during displacement reaction," *Chinese Rare Earths*, vol. 38, no. 6, pp. 57–63, 2017.

[19] Y. F. Xiao, Y. Y. Chen, Z. Y. Feng et al., "Leaching characteristics of ion-adsorption type rare earths ore with magnesium sulfate," *Transactions of Nonferrous Metals Society of China*, vol. 25, no. 11, pp. 3784–3790, 2015.

[20] Q. Li, Z. Y. He, Z. Y. Zhang et al., "Studies on coordination leaching of weathered crust elution-deposited rare earth ore with citrate," *Chinese Rare Earths*, vol. 36, no. 1, pp. 18–22, 2015.

[21] X. J. Wang, Y. L. Zhuo, K. Zhao et al., "Experimental measurements of the permeability characteristics of rare earth ore under the hydro-chemical coupling effect," *RSC Advances*, vol. 8, no. 21, pp. 11652–11660, 2018.

[22] G. Q. Deng and Y. M. Yang, "A review of the mining technologies of ion-absorbed rare earth mineral," *Chinese Rare Earths*, vol. 37, no. 3, p. 129, 2016.

[23] R. A. Chi, J. Tian, X. P. Luo, Z. G. Xu et al., "The basic research on the weathered crust elution-deposited rare earth ores," *Nonferrous Metals Science and Engineering*, vol. 3, no. 4, p. 1, 2012.

[24] R. A. Chi and J. Tian, *Weathered Crust Elution-Deposited Rare Earth Ores*, Nova Science Publishers, New York, NY, USA, 2008.

[25] K. P. Zhuo, J. L. Li, Y. J. Xu et al., "Experimental study of NMR characteristics in rock under freezing and thawing cycles," *Chinese Journal of Rock Mechanics and Engineering*, vol. 31, no. 4, p. 731, 2012.

[26] Q. Q. Huang, *Experimental study on permeability change rule of ion-absorbed rare-earth in ore leaching process*, Jiangxi University of Science and Technology, Ganzhou, China, 2014.